
# Comparison of morphological changes of corneal collagen fibers treated with collagen crosslinking agents using second harmonic generation images

Angel A. Zeitoune, Patrícia A. Bersanetti, Paulo Schor, Luciana A. Erbes, Carlos L. Cesar, Javier Adur

PII: S0141-8130(20)34506-2

DOI: https://doi.org/10.1016/j.ijbiomac.2020.09.147

Reference: BIOMAC 16777

To appear in: *International Journal of Biological Macromolecules*

Received date: 23 July 2020

Revised date: 18 September 2020

Accepted date: 19 September 2020

Please cite this article as: A.A. Zeitoune, P.A. Bersanetti, P. Schor, et al., Comparison of morphological changes of corneal collagen fibers treated with collagen crosslinking agents using second harmonic generation images, *International Journal of Biological Macromolecules* (2018), https://doi.org/10.1016/j.ijbiomac.2020.09.147

# Comparison of morphological changes of corneal collagen fibers treated with collagen crosslinking agents using second harmonic generation images

Angel A. Zeitoune[a], Patrícia A. Bersanetti[b], Paulo Schor[c], Luciana A. Erbes[a], Carlos L. Cesar[d,e] and Javier Adur[a]*

a-*Instituto de Investigación y Desarrollo en Bioingeniería y Bioinformática (IBB), UNER, CONICET, Oro Verde, Entre Ríos, Argentina, azeitoune@ingenieria.uner.edu.ar, lerbes@ingenieria.uner.edu.ar, jadur@ingenieria.uner.edu.ar;*

b-*Department of Biochemistry, Paulista School of Medicine, Federal University of São Paulo, São Paulo, Brazil, patricia.bersanetti@gmail.com;*

c-*Department of Ophthalmology and Visual Sciences, Paulista School of Medicine, Federal University of São Paulo, São Paulo, Brazil, paulo.schor@gmail.com;*

d-*Department of Physics of Federal University of Ceara (UFC), Brazil, ;*

e-*INFABiC - National Institute of Science and Technology on Photonics Applied to Cell Biology, Campinas, Brazil,*

* Corresponding author: Javier Adur

Address: Ruta prov 11 km 10, Oro Verde, Entre Ríos, Argentina; e-mail: jadur@ingenieria.uner.edu.ar; Tel. +54 343 4975100; Fax: +54 343 4975077.

**Abstract**

Corneal cross-linking (CXL) is a common surgical procedure used to modify corneal biomechanics and stabilize keratoconus progression which is still under discussion. Its side effects, which are mostly related to anatomical unpredictability and stromal exposure, are the reason for the search for new CXL agents. In this work we have quantitatively evaluated the porcine corneal stroma architecture treated with collagen crosslinking agents such as riboflavin solutions and açai extract, using second harmonic generation microscopy. Aimed at evaluating the morphological changes in the corneal stroma after collagen crosslinking under a CXL chemical agent, a tubeness filter based Hessian matrix to obtain a 3D fiber characterization of the SHG images was applied. The results showed a curling effect and shortening of the collagen fibers treated with açai as compared to the control. They also showed a higher degree of clustering of the collagen fibers with larger empty spaces when compared to the other two groups. We believe that studies such as these presented in this paper are a good direct nondestructive and free labeling evaluation technique that allows the observation of morphologic features of corneas treated with new CXL agents.



Keywords: collagen, crosslinking, SHG (Second Harmonic Generation)

## 1. Introduction

Keratoconus (KC) is an eye disorder associated with structural changes in the organization of corneal collagen. This pathology develops a progressive deformation and thinning of the cornea. It has inflammatory hallmarks and may result in irregular astigmatism that leads to blurry vision, double vision and light sensitivity [1]. Early stages or non-severe cases benefit from spectacles or contact lenses, but as the corneal curvature progresses, surgical interventions such as intracorneal rings or transplants might be needed to restore vision. Chemical surgeries such as the conventional or Dresden protocol corneal crosslinking, induced by UVA light at 365 nm using an irradiance of 3 mWcm-2 and 0.1% riboflavin instillation for 30 minutes are effective allowing time for intervention, which can slow down or outright halt the progression of the disease in the majority of cases [2,3]. The photochemical process creates additional chemical bonds within the tissue, thereby increasing the mechanical and biochemical stability of the treated corneas [4-6]. Side effects which are mostly related to anatomical unpredictability and stromal exposure (oxidation damage, inflammation, infection) are the reason for the search of new CXL agents. Faster and less complicated methods that do not require irradiation have been proposed as natural agents such as açaí. They have been proven to be very efficient in promoting in vitro crosslinking in the corneal tissue. Moreover, previous results have showed that açai extract is efficient at promoting a significant increase in the elastic modulus of corneas. The elastic modulus was 10.5 times higher in corneas treated with 4% açaí extract for 2h than in those in the control group [7].

Even with growing acceptance and promising results, CXL faces major challenges since there is no method to objectively measure or image the effects of the treatment and its

potential side effects due to the oxidative consequences to the nearby tissue [8] and biomechanical predictability.

To evaluate the effectiveness of corneal CXL, many clinical (visual acuity, slit lamp examination, optical coherence tomography, and confocal microscopy) [9-13] and laboratory (stress–strain behavior, enzymatic digestion and hydration treatment) [14] techniques have been applied. Clinical results represent and partially quantify the effectiveness of corneal CXL in an indirect way. Despite advances in clinical and biochemical studies of the effects of corneal CXL, the direct nondestructive observation of morphologic features of corneas after CXL treatment without extrinsic labeling is necessary. To tackle this problem, in recent years, second harmonic generation (SHG) microscopy has become a valid alternative [15-18].

Being intrinsically non-centrosymmetric, specific types of collagen fibers generate a SHG signal when illuminated by a high intensity femtosecond-pulsed laser [19]; the emitted signal is at half the wavelength of the incident optical beam. Since the generation is confined to a sub-femtoliter focal volume, SHG microscopy permits 3D imaging [20,21]. As a result, this technique has become an important aspect of both qualitative and quantitative studies of collagen-based tissues [22-25].

The cornea has been analyzed with SHG microscopy by many different authors in a number of animal models (including humans) under several experimental conditions [26]. Corneal collagen is organized in a depth- dependent fashion [27] and collagen fibers always show a regular packaging [27,28]. However, this regular pattern has been shown to change with pathologies [29], including keratoconus [30,31], after surgical procedures [32], and after CXL treatment [4]. Due to this, both classification and quantification of collagen arrangement might be a powerful tool in biomedicine as well as in medical studies.

In order to extract meaningful collagen fiber information, researchers have developed several segmentation methods. These methods are based on the application of filters such as Gaussian, SPIRAL-TV, Tubeness, and curvelet-denoising [33]. Collagen fibers that have been extracted may be evaluated, allowing to quantify geometrical properties and to compute the degree of organization in corneal collagen in the presence of pathologies [34] or after physical damage [35,36]. Although there are a number of 2D approaches developed for collagen fiber orientation analysis, only a small number of 3D techniques exist to quantify fiber distribution in an image stack.

Aimed at evaluating the morphological changes in the corneal stroma after collagen crosslinking under a CXL chemical agent (açai), this work applied a tubeness filter based Hessian matrix to obtain a 3D fiber characterization of SHG images.

## 2. Materials and Methods

### *2.1 Sample preparation*

All the steps of this study were approved by the UNIFESP Ethical Committee (CEP 0580/10) University of Sao Paulo. Throughout all the procedures, the ARVO Statement for the Use of Animals in Ophthalmic and Vision Research was used. Riboflavin (0.1%; 10 mg riboflavin-5-phosphate in 10 mL dextran T-500 20%) was purchased from Ophthalmos Laboratories (São Paulo, Brazil). The açai extract was supplied by Gamma (São Paulo, Brazil). Enucleated porcine eyes with clear corneas were obtained from the abattoir within less than 6 h postmortem.

### *2.2 Corneal Crosslinking Procedures*

Six porcine eyes were mechanically de-epithelized and then trephined (12 mm). The corneas were divided in half and each of them separated into three groups: açai (n=3), riboflavin (n=3) and control group (n=6). The first one was completely immersed in 4% açai solution for 2 h. The riboflavin CXL methodology consisted in dripping

0.1% riboflavin metilcelulose solution every 5 minutes, for 30 min on the corneas, followed by the application of UV light at 365 nm for 30 min (with instillation of riboflavin every 5 min during UV light stimulation), using a solid-state device X-Link (Opto Electronics, São Carlos, Brazil). Specimens of the three groups were maintained in Optisol-GS storage media (Bausch & Lomb, Irvine, California, USA) until the time for microscopy analysis.

***2.3 SHG Microscopy***

SHG microscopy analysis was performed at Biomedical Lasers Application Laboratory of the Institute of Physics, State University of Campinas. The samples were mounted with the corneal surface parallel to the scanning laser plane and with their anterior face down. The corneas were observed under a 40× magnification in the microscope, LSM 780 NLO (Carl Zeiss, Germany). The optimal wavelength of the generation of second-harmonic signals from the corneal collagen was found to be 800 nm. Forward scatter signals that passed through the tissue were collected. The data sets were analyzed using an image browser, Zeiss LSM Image Examiner (Carl Zeiss, Germany).

***2.4 Image acquisition***

Images of 73.29 x 73.29 $\mu m^2$ with a resolution of 512 x 512 pixels used in our experiment were selected to analyze collagen distribution. A z-stack of each sample of SHG images was taken with 21 optical sections with 1 μm steps between each section. Six eyes were divided in half and twelve cornea halves were analysed in total. Six untreated halves were used as control and three were treated with açai aqueous solution. The other three halves were treated with riboflavin and used as reference. Figure 1 shows representative images of each condition.

Two methods were used to quantify the characteristics of the collagen fibers: analysis of geometrical properties of each individual fiber and fibers distribution.

### *2.5 Segmentation*

Each image was filtered with a 3x3x1 mean filter to smooth the image, to reduce the amount of intensity variation and enhance continuous collagen fibers intensity (Fig. 2A). Then, a ridge detection based on a multi-scale line filter designed by Sato et al [37] calculated a second order derivative matrix based on the Hessian matrix:

$$H(x,y) = \begin{pmatrix} \frac{\partial^2 g}{\partial x^2} & \frac{\partial^2 g}{\partial x \partial y} \\ \frac{\partial^2 g}{\partial x \partial y} & \frac{\partial^2 g}{\partial y^2} \end{pmatrix} \quad (1)$$

Eigenvalues and eigenvectors were calculated for each element of the Hessian matrix. The magnitude and the sign of the eigenvalues were used to construct a new intensity image (Fig. 2B). A global image threshold based on Otsu's method was applied (Fig 2C). Since many collagen fibers are very close together, an algorithm based on eigenvectors was used to eliminate connectivity. Figure 3 shows the detail of detached fibers. Finally, a skeletonized image was created where all small branches had been removed (Fig 2D).

### *2.6 Geometrical properties*

The morphological changes of collagen fibers using first-order statistics were quantified measuring density, length, size, sinuosity and curvature. The density is the amount of collagen fibers per unit volume. In this case, the amount of collagen fibers per 1000 $\mu m^3$. The length of the fiber is found by summing the distance of each pair of points that belong to the fiber skeleton. Size is the sum of the amount of points. Sinuosity is measured by the relationship between the length of the fiber and the distance in a straight line between the ends. Curvature is measured by the relationship between the fiber centroid and the distance in a straight line between the ends.

### *2.7 Fibers distribution*

Once we had obtained the segmentation of all the fibers with their spatial location, we analyzed how these were distributed. To do this we extracted two factors. One calculates the distance of each fiber with its neighbor and the second the maximum distance between neighboring fibers. The first was calculated by means of the nearest neighbor algorithm. A cumulative distribution function plot was built and a nonparametric fit coefficient was calculated to characterize the clustering. This parameter provided an idea of how the fibers are grouped in clusters. The second one, thinking in reverse, is looking at the void space between the collagen fiber bundles.

## 3. Results

The SHG images show notable differences between normal and CXL treated corneas (Fig. 1) such as compaction, length and distribution of the collagen fibers after both açai and riboflavin CXL procedures. In order to demonstrate these differences, segmentation of the collagen fibers was carried out. Segmentation resulted in a skeletonized representation of the collagen fibers. Figure 4 shows the superposition of skeletonized collagen fibers in the original image in one layer for each of the types of samples (control, with açai, and with riboflavin). Red lines represent the path of skeletonized fibers. It can be seen that this path accompanies the trajectory of the fiber. The results obtained indicate that collagen fibers have been well represented. If all the layers are stacked (twenty-one images separated by one μm each), a three-dimensional representation of each sample is obtained (Fig. 5). Red lines represent the path of skeletonized fibers in the most superficial layer and blue lines represent the path of skeletonized fibers in the deepest one.

Having a good location of each fiber allows the calculation of better numerical indicators that represent the tissue. Table 1 summarizes the results of the geometric

properties and the distribution of collagen fibers. As can be seen, collagen fibers treated with açai have greater differences with respect to control samples than those treated with riboflavin. It mainly shows that the fibers treated with açai are shorter and more curved. Plotting amount of fibers as a function of length, a downward curve can be obtained (curve not showed). Defining an arbitrary classification threshold (within a wide range, 4 µm to 12 µm) between short fibers and long fibers of 10 µm, we can count the amount of long and short fibers that each image has. The amount of collagen fibers treated with açai that have a length bigger than 10 µm is 69.3 ± 19.5 while in the case of the control group it is 333.0 ± 52.2. In fibers treated with riboflavin the amount is 278.3 ± 56.8. This result shows that the fibers treated with açai have shorter fibers than those in the control samples. This short/large relationship is maintained even by changing the threshold value. The shortening of the fibers occurs due to the folding, without loss of structure. In the crosslinking process using acai, a shortening of the collagen is evident which may be attributed to a folding of the fibers in a wave shape without the occurrence of a break of the protein chains [38].

The clustering is quantized by measuring the distance between each collagen fiber with its neighbor. The second clustering factor measures the space between the collagen fibers. Both parameters show bigger clustering in samples treated with açai.

**Discussion**

CXL altered the natural history of keratoconus, the leading cause of corneal transplants worldwide. Several children and teenagers have been spared of corneal rejection, permanent use of contact lenses and long recovery time [39]. Complications such as corneal melting and progressive flattering of the anterior corneal curvature are present in the literature [40] and partially explain the search for alternatives to the conventional Dresden protocol. Fast, epi-on, ultra-fast CXL options are currently under trial and their

efficacy is expected to be just enough to slow the progression of the disease, but can be associated with some complications and failure [41]. Ultra-fast is one of the strategies that use greater power and shorter exposure time. This option has been theoretically used with less biomechanical effects, but produce less structural modification in the cornea, such as progressive corneal flattening [42].

Non UV-based treatments potentially spare adjacent tissue from oxidative stress involved in the process, allowing for treatment in thin corneas. Natural agents also may be applied overnight or daily, at home or in the office. Doses and delivery strategies might further democratize the access and spare even more people from complications.

This scenario justifies the search for direct, non-destructive, objective methods of tissue evaluation, under different chemical agents CXL protocols, along with biocompatibility (to be further studied).

The arrangement of the collagen fibers in the corneal stroma follows principally an arrangement parallel to the surface, with few perpendicular fibers in humans [43]. We have detected a shortening of the fibers that may explain the corneal flattening found in some patients treated with CXL (mainly conventional), which until now had no satisfactory explanation. This effect must be quantified, predicted and used in order to build a more precise model to reach the final refractive result of the procedure. With this quantification, it is expected that the therapeutic treatment (which seeks to decrease the rate of progression of the disease) also has a refractive purpose (improving the patient's vision by decreasing the corneal curvature). The higher value of the space between the collagen fibers observed in the corneas subjected to CXL can be attributed to the clustering of collagen fibers.

CXL using extract of Euterpe oleracea (açai), a fruit obtained from a palm tree that is found in the northern states of Brazil, showed more intense fiber curling and clustering.

These effects observed in the three-dimensional quantification can be due to the observation process and to the molecular structure of açai. In the former case, fibers can weave in and out of the focal plane (fibers changing direction and diving in and out of the observation plane) and appear shorter. Probably, the fibrils are curling in response to acai extract exposure. This is happening on a nanometer scale and is not directly visible to SHG, but has a knock-on effect on the much larger fibers, which are visible in the en face images scans. If the curling of the nanoscopic fibrils is causing the fibers themselves to curl, essentially creating a sinusoidal pattern with a shorter "wavelength" than before, then the fibers would appear shorter in the en-face images. On the other hand, various polyphenolic compounds, such as proanthocyanidin (condensed tannins) are present in açai. These molecules can exhibit the potential to promote stable hydrogen-bonded structures formed between the carbonyl groups of the amino acids of the collagen fibrils and the hydroxyl groups of the polyphenols. Proanthocyanidins are molecules of varying size and structure that act by intra and interfibrillar interaction. In the interfibrillar space, the molecules must replace the water of hydration and by their size an increase in the distance between the fibers of collagen is expected. The spacing between fibers is not related to a hydrogen bond, but is due to the insertion of proanthocyanidins which, through interaction with hydrogen, remain in place. Then, the increased stability of the corneas subjected to CXL can be attributed to new hydrophobic interactions between the collagen fibers, which can be established in the CXL by molecules present in the açai extract [5].

Since açai extract possesses different size molecules, it is possible that a heterogeneity of reactions occurs in different parts of the tissue. That may be a marker for the non-purity of the extract that shall be further characterized and defined. Homogeneous molecules will induce predictable and uniformly distributed effects.

Although future studies with more samples are needed, in these preliminary results the curling effect and fiber shortening under the effects of açai extract are remarkable. This further corroborates our finding that this substance (proanthocyanidin) is a strong candidate for CXL even under smaller concentrations. The advantage of the acai methodology over CXL with UV radiation is related to the formation of free radicals, due to riboflavin photo-stimulation and the toxicity already demonstrated from this oxidation process in the cellular membrane, leading to its destruction. This principle does not occur in the chemical basis of açai action. Therefore, less toxicity and damage to cells as sensitive as endothelia cells is expected. This is an important factor fact as these cells do not reproduce and their destruction may cause bully keratopathy and a consequential need for cornea transplantation.

Another important aspect to highlight is that the use of natural products, that do not require photoactivation, could be applied in the form of eye drops or ointments, through controlled release, to be used by patients in everyday life. Then, this strategy would reduce risks and discomfort associated with corneal chemical surgery currently required for the CXL performance. In addition, dose control and greater effect can be used in more serious cases, besides progressive corneal thinning arising from infectious necrosis.



## CONCLUSION

We have quantitatively evaluated the morphological changes in the corneal stroma architecture, using second harmonic generation microscopy, after treatment with collagen crosslinking agents such açai extract. Using a tubeness filter based on the Hessian matrix to obtain a 3D fiber characterization, we observed a curling effect and fiber shortening after açai applications. In addition, a higher degree of clustering of the

collagen fibers with larger empty spaces was detected. However, further studies need to be carried out to prove the concept of clustering and titer the dose related to stromal (biomechanical) and superficial (curvature) effects, along with biocompatibility of fractions to be extracted from the natural plant source. We believe that these studies should be validated with three-dimensional quantification procedures (nondestructive and free labeling) such as those presented in this paper.

**Funding and acknowledgements**: This work was supported by grant of IBB-CONICET UNER for funding (PIO Res: 4337/15; Contract grant number: N8 14320140100004 CO).
The authors also acknowledge the English language editing service provided by Prof. Diana Waigandt (Área de Asesoramiento Interdisciplinar - Facultad de Ingeniería - Universidad Nacional de Entre Ríos).

## Author contributions

**A.A.Z**: Methodology, Software, Validation, Writing original draft; **P.A.B**: Conceptualization, Methodology, Investigation; **P.S:** Conceptualization, Methodology, Formal analysis, Investigation; **L.A.E:** Software, Formal analysis**; C.L.C:** Conceptualization, Formal analysis, Visualization, **J.A:** Formal analysis, Investigation, Writing and Editing.

### Declaration of competing interest

All authors declare no conflict of interest.

## References

1. Romero-Jiménez M, Santodomingo-Rubido J, and Wolffsohn JS. Keratoconus: A review. Cont Lens Anterior Eye. 2010;33:157–66. doi:10.1016/j.clae.2010.04.006.
2. Wollensak G, Spoerl E, Seiler T. Riboflavin/ultraviolet-a-induced collagen crosslinking for the treatment of keratoconus. Am J Ophthalmol. 2003;135:620–27. doi:10.1016/s0002-9394(02)02220-1.

3. Spoerl E, Huhle M, Seiler T. Induction of cross-links in corneal tissue. Exp Eye Res. 1998;66:97–103. doi:10.1006/exer.1997.0410.
4. Tan HY, Chang YL, Lo W, Hsueh CM, Chen WL, Ghazaryan AA, Hu PS, Young TH, Chen SJ, Dong CY. Characterizing the morphologic changes in collagen crosslinked–treated corneas by Fourier transform–second harmonic generation imaging. J Cataract Refract Surg. 2013;39:779–88. doi:10.1016/j.jcrs.2012.11.036.
5. Ávila FJ, Artal P, Bueno JM. Quantitative Discrimination of Healthy and Diseased Corneas with Second Harmonic Generation Microscopy. Transl Vis Sci Technol. 2019; 8:51. doi: 10.1167/tvst.8.3.51.
6. Bueno JM, Ávila FJ, Martínez-García MC. Quantitative Analysis of the Corneal Collagen Distribution after *In Vivo* Cross-Linking with Second Harmonic Microscopy. Biomed Res Int. 2019; 2019:3860498 doi: 10.1155/2019/3860498.
7. Bersanetti PA, Bueno TLN, Morandim-Giannetti A, Nogueira RF, Matos JR, Schor P. Characterization of rabbit corneas subjected to stromal stiffening by the açai extract (euterpe oleracea). Curr Eye Res. 2016;42:528–33. doi:10.1080/02713683.2016.1214970.
8. Hafezi F, Kanellopoulos J, Wiltfang R, Seiler T. Corneal collagen crosslinking with riboflavin and ultraviolet A to treat induced keratectasia after laser in situ keratomileusis. J Cataract Refract Surg. 2007;33:2035-40. doi:10.1016/j.jcrs.2007.07.028.
9. Seiler T, Hafezi F. Corneal cross-linking-induced stromal demarcation line. Cornea. 2006;25:1057-59. doi:10.1097/01.ico.0000225720.38748.58.
10. Doors M, Tahzib NG, Eggink FA, Berendschot TTJM, Webers CAB, Nuijts RMMA. Use of anterior segment optical coherence tomography to study corneal changes after collagen cross-linking. Am J Ophthalmol. 2009;148:844-51.e2. doi:10.1016/j.ajo.2009.06.031.
11. Mazzotta C, Traversi C, Baiocchi S, Caporossi O, Bovone C, Sparano MC, Balestrazzi A, Caporossi A. Corneal healing after riboflavin ultraviolet-A collagen cross-linking determined by confocal laser scanning microscopy in vivo: early and late modifications. Am J Ophthalmol. 2008;146:527–33.e1. doi:10.1016/j.ajo.2008.05.042.

12. Spoerl E, Schreiber J, Hellmund K, Seiler T, Knuschke P. Studies on the stabilization of the cornea in rabbits. Ophthalmologe. 2000;97:203–6. doi:10.1007/s003470050515.
13. Yuksel E, Cubuk MO, Yalcin NG. Accelerated epithelium-on or accelerated epithelium-off corneal collagen cross-linking: Contralateral comparison study. Taiwan J Ophthalmol. 2020;10(1):37-44. doi: 10.4103/tjo.tjo_11_19.
14. Wollensak G, Aurich H, Pham DT, Wirbelauer C. Hydration behavior of porcine cornea crosslinked with riboflavin and ultraviolet A. J Cataract Refract Surg. 2007;33:516–21. doi:10.1016/j.jcrs.2006.11.015.
15. Steven P, Hovakimyan M, Guthoff RF, Hüttmann G, Stachs O. Imaging corneal crosslinking by autofluorescence 2-photon microscopy, second harmonic generation, and fluorescence lifetime measurements. J Cataract Refract Surg. 2010;36:2150–59. doi:10.1016/j.jcrs.2010.06.068.
16. Campagnola, PJ, Loew LM. Second-harmonic imaging microscopy for visualizing biomolecular arrays in cells tissues and organisms. Nat Biotechnol. 2003;21:1356–60. doi:10.1038/nbt894.
17. Ogura Y, Tanaka Y, Hase E, Yamashita T, Yasui T.Exp Dermatol.Texture analysis of second-harmonic-generation images for quantitative analysis of reticular dermal collagen fiber in vivo in human facial cheek skin. Exp Dermatol. 2019; 28(8):899-905. doi: 10.1111/exd.13560.
18. Zyablitskaya M, Munteanu EL, Nagasaki T, Paik DC. Second Harmonic Generation Signals in Rabbit Sclera As a Tool for Evaluation of Therapeutic Tissue Cross-linking (TXL) for Myopia. J Vis Exp. 2018; (131):56385. doi: 10.3791/56385.
19. Morishige N, Takagi Y, Chikama TI, Takahara A, Nishida T. Three-dimensional analysis of collagen lamellae in the anterior stroma of the human cornea visualized by second harmonic generation imaging microscopy. Invest Ophthalmol Vis Sci. 2011;52:911. doi:10.1167/iovs.10-5657.
20. Pena AM, Fabre A, Débarre D, Marchal-Somme J, Crestani B, Martin JL, Beaurepaire E, Schanne-Klein MC. Three-dimensional investigation and scoring of extracellular matrix remodeling during lung fibrosis using multiphoton microscopy. Microsc Res Tech. 2007;70:162–70. doi:10.1002/jemt.20400.

21. Chen X, Nadiarynkh O, Plotnikov S, Campagnola PJ. Second harmonic generation microscopy for quantitative analysis of collagen fibrillar structure. Nat Protoc. 2012;7:654–69. doi:10.1038/nprot.2012.009.
22. Zeitoune AA, Luna JSJ, Salas KS, Erbes L, Cesar CL, Andrade LALA, Carvahlo HF, Bottcher-Luiz F, Casco VH, Adur J. Epithelial ovarian cancer diagnosis of second-harmonic generation images: a semiautomatic collagen fibers quantification protocol. Cancer Inform. 2017;16:117693511769016. doi:10.1177/1176935117690162.
23. Bueno JM, Gualda EJ, Artal P. Analysis of corneal stroma organization with wavefront optimized nonlinear microscopy. Cornea. 2011;30:692–701. doi:10.1097/ico.0b013e3182000f94.
24. Bueno JM, Ávila FJ, Hristu R, Stanciu SG, Eftimie L, Stanciu GA. Objective analysis of collagen organization in thyroid nodule capsules using second harmonic generation microscopy images and the Hough transform. Appl Opt. 2020;59(23):6925-6931. doi: 10.1364/AO.393721.
25. Castor MDGFC, Torres LC, Mello PJV, Natal RA, Vassallo J. Study on collagen parameters in vulvar cancer and preneoplastic lesions by Second Harmonic Generation microscopy. Sci Rep. 2020;10(1):5568. doi: 10.1038/s41598-020-62340-3.
26. Teng SW, Tan HY, Peng JL, Lin HH, Kim KH, Lo W, Sun Y, Lin WC, Lin SJ, Jee SH, et al. Multiphoton autofluorescence and second-harmonic generation imaging of the ex vivo porcine eye. Invest Ophthalmol Vis Sci. 2006;47:1216. doi:10.1167/iovs.04-1520.
27. Han M, Giese G, Bille JF. Second harmonic generation imaging of collagen fibrils in cornea and sclera. Opt Express. 2005;13:5791. doi:10.1364/opex.13.005791.
28. Hsueh CM, Lo W, Chen WL, Hovhannisyan VA, Liu GY, Wang SS, Tan HY, Dong CY. Structural characterization of edematous corneas by forward and backward second harmonic generation imaging. Biophys J. 2009;97:1198–1205. doi:10.1016/j.bpj.2009.05.040.
29. Tan HY, Sun Y, Lo W, Lin SJ, Hsiao CH, Chen YF, Huang SCM, Lin WC, Jee SH, Yu HS, et al. Multiphoton fluorescence and second harmonic generation

imaging of the structural alterations in keratoconus ex vivo. Invest Ophthalmol Vis Sci. 2006;47:5251. doi:10.1167/iovs.06-0386.

30. Morishige N, Wahlert AJ, Kenney MC, Brown DJ, Kawamoto K, Chikama T, Nishida T, Jester JV. Second-harmonic imaging microscopy of normal human and keratoconus cornea. Invest Ophthalmol Vis Sci. 2007;48:1087. doi:10.1167/iovs.06-1177.
31. Araki-Sasaki K, Osakabe Y, Fujita K, Miyata K, Hirano K. Collagen fiber changes related to keratoconus with secondary corneal amyloidosis. Int Med Case Rep J. 2018; 11:193-199. doi: 10.2147/IMCRJ.S162655.
32. Bueno JM, Gualda EJ, Giakoumaki A, Pérez-Merino P, Marcos S, Artal P. Multiphoton microscopy of ex vivo corneas after collagen cross-linking. Invest Ophthalmol Vis Sci. 2011;52:5325. doi:10.1167/iovs.11-7184.
33. Bredfeldt, JS, Liu Y, Pehlke CA, Conklin MW, Szulczewski JM, Inman DR, Keely PJ, Nowak RD, Mackie TR, Eliceiri KW. Computational segmentation of collagen fibers from second-harmonic generation images of breast cancer. J Biomed Opt. 2014;19:016007. doi:10.1117/1.jbo.19.1.016007.
34. Lo W, Chen WL, Hsueh CM, Ghazaryan AA, Chen SJ, Ma DHK, Dong CY, Tan HY. Fast fourier transform based analysis of second-harmonic generation image in keratoconic cornea. Invest Ophthalmol Vis Sci. 2012 53 (7): 3501. doi:10.1167/iovs.10-6697.
35. Matteini P, Ratto F, Rossi F, Cicchi R, Stringari C, Kapsokalyvas D, Pavone FS, Pini R. Photothermally-induced disordered patterns of corneal collagen revealed by SHG imaging. Opt Express. 2009;17:4868. doi:10.1364/oe.17.004868.
36. Hanley CJ, Noble F, Ward M, Bullock M, Drifka C, Mellone M, Manousopoulou A, Johnston HE, Hayden A, Thirdborough S, et al. A subset of myofibroblastic cancer-associated fibroblasts regulate collagen fiber elongation, which is prognostic in multiple cancers. Oncotarget. 2016;7:6159-6174. doi:10.18632/oncotarget.6740.
37. Sato Y, Nakajima S, Shiraga N, Atsumi H, Yoshida S, Koller T, Gerig G, Kikinis R. Three-dimensional multi-scale line filter for segmentation and visualization of curvilinear structures in medical images. Med Image Anal. 1998;2:143–68. doi:10.1016/S1361-8415(98)80009-1.

38. Tan HY, Chang YL, Lo W, Hsueh CM, Chen WL, Ghazaryan AA, Hu PS, Young TH, Chen SJ, Dong CY. Characterizing the morphologic changes in collagen crosslinked-treated corneas by Fourier transform-second harmonic generation imaging. J Cataract Refract Surg. 2013; 39(5):779-88. doi: 10.1016/j.jcrs.2012.11.036.

39. Poli M, Cornut PL, Balmitgere T, Aptel F, Janin H, Burillon C. Prospective study of corneal collagen cross-linking efficacy and tolerance in the treatment of keratoconus and corneal ectasia. Cornea. 2013;32:583–90. doi:10.1097/ico.0b013e31825e8414.

40. Noor IH, Seiler TG, Noor K, Seiler T. Continued long-term flattening after corneal cross-linking for keratoconus. J Refract Surg. 2018;34:567–70. doi:10.3928/1081597x-20180607-01.

41. Zhang X, Zhao J, Li M, Tian M, Shen Y, Zhou X. Conventional and transepithelial corneal cross-linking for patients with keratoconus. PLoS ONE. 2018;13:e0195105. doi:10.1371/journal.pone.0195105.

42. Wen D, Li Q, Song B, Tu R, Wang Q, O'Brart DPS, McAlinden C, Huang J. Comparison of Standard Versus Accelerated Corneal Collagen Cross-Linking for Keratoconus: A Meta-Analysis. Invest Ophthalmol Vis Sci. 2018; 59(10): 3920-3931. doi: 10.1167/iovs.18-24656.

43. Winkler M, Shoa G, Xie Y, Petsche SJ, Pinsky PM, Juhasz T, Brown DJ, Jester JV. Three-dimensional distribution of transverse collagen fibers in the anterior human corneal stroma. Invest Ophthalmol Vis Sci. 2013;54:7293. doi:10.1167/iovs.13-13150.

**Table 1:** Descriptive results of the geometric properties and fibers distribution for different samples.

| | Control (n=6) | Açaí (n=3) | Riboflavin (n=3) |
|---|---|---|---|
| **Geometric properties** | | | |
| Density | 6.4 ± 0.2 | 4.5 ± 0.7 | 6.2 ± 0.4 |
| Length | 5.0 ± 3.1 | 4.1 ± 1.9 | 4.9 ± 2.9 |
| Size | 4.5 ± 2.3 | 3.7 ± 1.7 | 4.4 ± 2.5 |
| Sinuosity | 1.1 ± 0.3 | 1.1 ± 0.5 | 1.1 ± 0.4 |
| Curvature | 0.1 ± 0.2 | 0.2 ± 0.3 | 0.1 ± 0.2 |
| **Threshold 8 µm** | | | |
| Amount of long collagen fibers | 613.4 ± 51.4 | 180.3 ± 48.9 | 542.3 ± 100.4 |
| Amount of short collagen fibers | 4397.6 ± 275.4 | 3325.7 ± 667.1 | 542.3 ± 333.1 |
| Relation (short/large) | 7.2 | 18.4 | 8.0 |
| **Threshold 10 µm** | | | |
| Amount of long collagen fibers | 333.0 ± 52.2 | 69.3 ± 19.5 | 278.3 ± 56.8 |
| Amount of short collagen fibers | 4678.0 ± 275.0 | 3436.7 ± 698.0 | 4588.0 ± 376.8 |
| Relation (short/large) | 14.0 | 49.6 | 16.5 |
| **Threshold 12 µm** | | | |
| Amount of long collagen fibers | 186.4 ± 53.8 | 29.3 ± 5.5 | 151.0 ± 47.3 |
| Amount of short collagen fibers | 4824.5 ± 277.2 | 3476.7 ± 708.1 | 4715.3 ± 387.2 |
| Relation (short/large) | 25.9 | 118.5 | 31.2 |
| **Fibers distribution** | | | |
| Clustering coeficient | 8.0 ± 0.8 | 9.0 ± 1.3 | 7.6 ± 0.1 |
| Maximum distance between collagen fibers [µm] | 2.9 ± 0.4 | 6.3 ± 1.9 | 3.1 ± 0.7 |

**Legends**

**Figure 1**: Representative maximum projection (stack of 21 images 1 µm steps between each section) of normal (A) and CXL treated (B, C) corneas. Normal (A), açaí (B), riboflavin (C). Scale bars: 10 µm.

**Figure 2**: Steps of the segmentation process of collagen fibers. (A) Filtered image with a mean filter. (B) Ridge detection using Hessian matrix. (C) Thresholded image using Otsu's method. (D) Skeletonized fibers (red) superimposed on the original image. Scale bars: 10 µm.

**Figure 3**: Detail of the result of detached algorithm that allows to separate the collagen fibers very close together. Before (A) and After (B) the application of the algorithm. Scale bars: 10 µm.

**Figure 4**: Representative Skeletonized fibers superimposed on the original image for each sample type. Control (A), açaí (B) and riboflavin (C). Red lines represent the path of skeletonized collagen fibers after segmentation. Scale bars: 10 µm.

**Figure 5**: Representative 3D representation (73µm x 73µm x 21µm) of collagen fibers segmentation. Control (A), açaí (B) and riboflavin (C). Red lines represent the path of skeletonized fibers in the superficial layer and blue lines represent the path of skeletonized fibers in the deepest layer. In the right side of the pictures, 3D ROI (21µm x 21µm x 21µm) highlight visual fiber collagen distribution.

Comparison of morphological changes of corneal collagen fibers treated with collagen crosslinking agents using second harmonic generation images

Angel A. Zeitoune, Patrícia A. Bersanetti, Paulo Schor, Luciana A. Erbes, Carlos L. Cesar and Javier Adur

**Declaration of competing interest**

All authors declare no conflict of interest.

**Credit Author Statement**

## Author contributions

**A.A.Z**: Methodology, Software, Validation, Writing original draft; **P.A.B**: Conceptualization, Methodology, Investigation; **P.S:** Conceptualization, Methodology, Formal analysis, Investigation; **L.A.E:** Software, Formal analysis**; C.L.C:** Conceptualization, Formal analysis, Visualization, **J.A:** Formal analysis, Investigation, Writing and Editing.

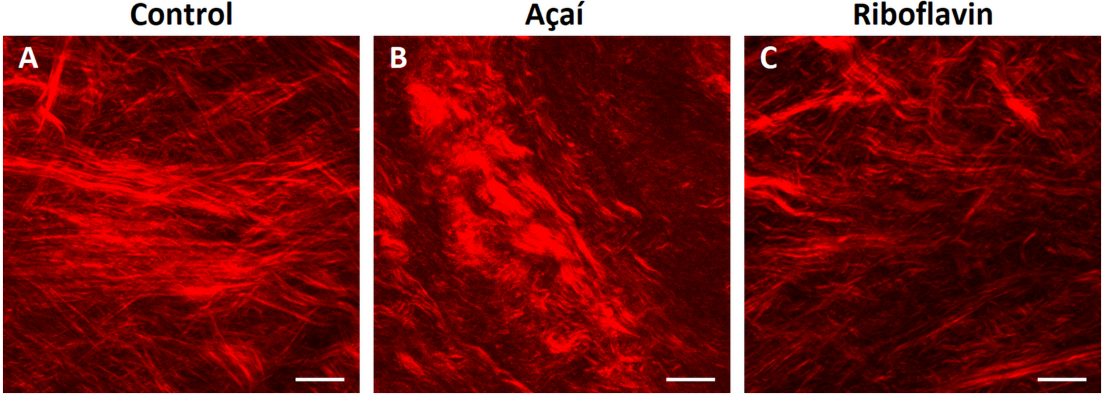


Figure 1

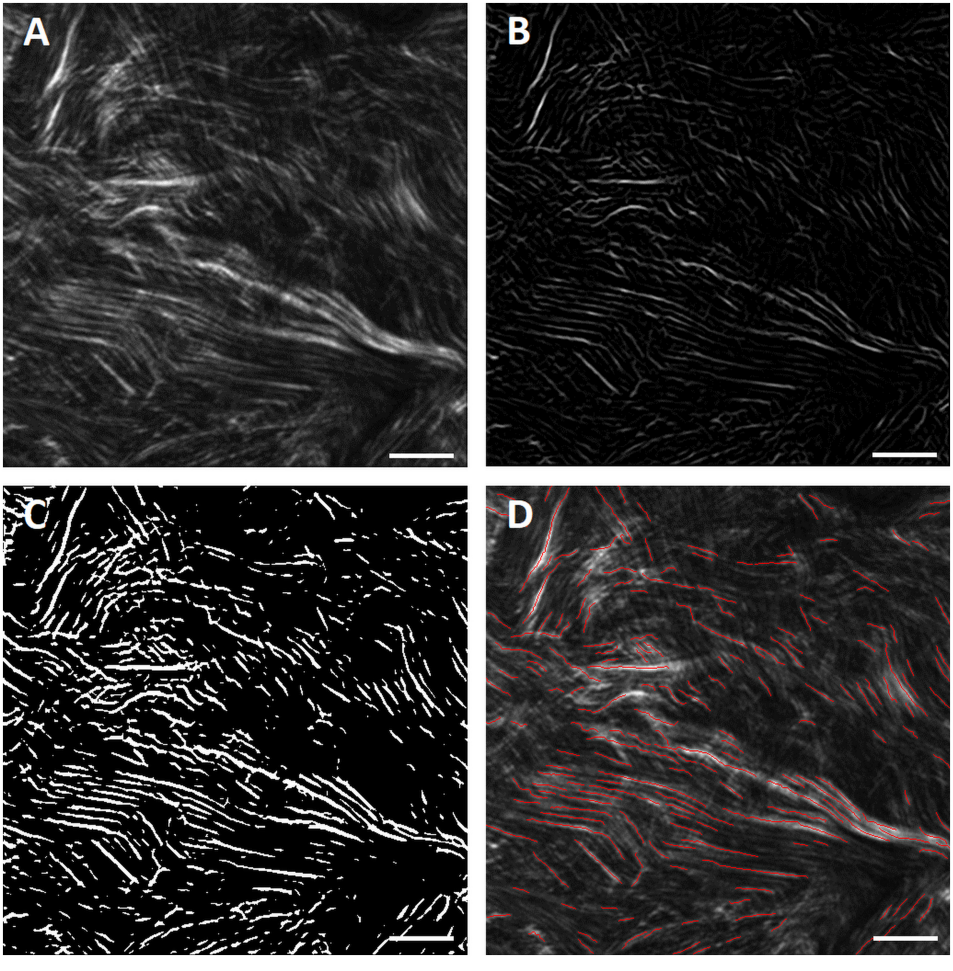


Figure 2

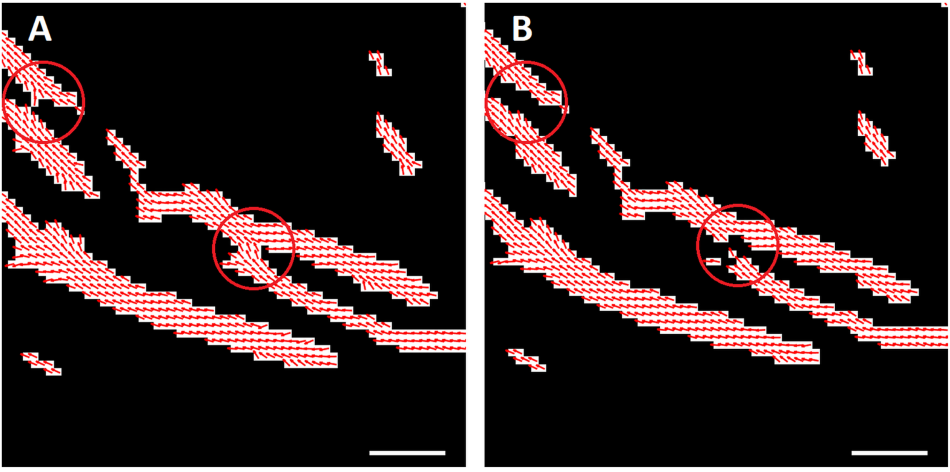


Figure 3

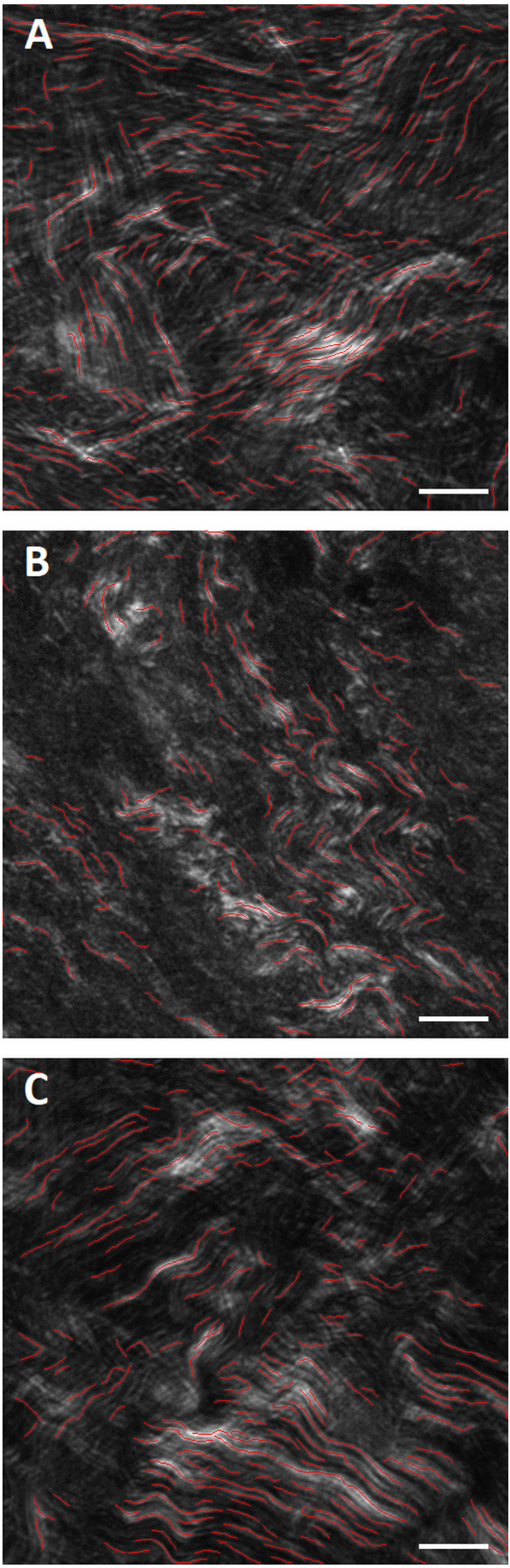


Figure 4

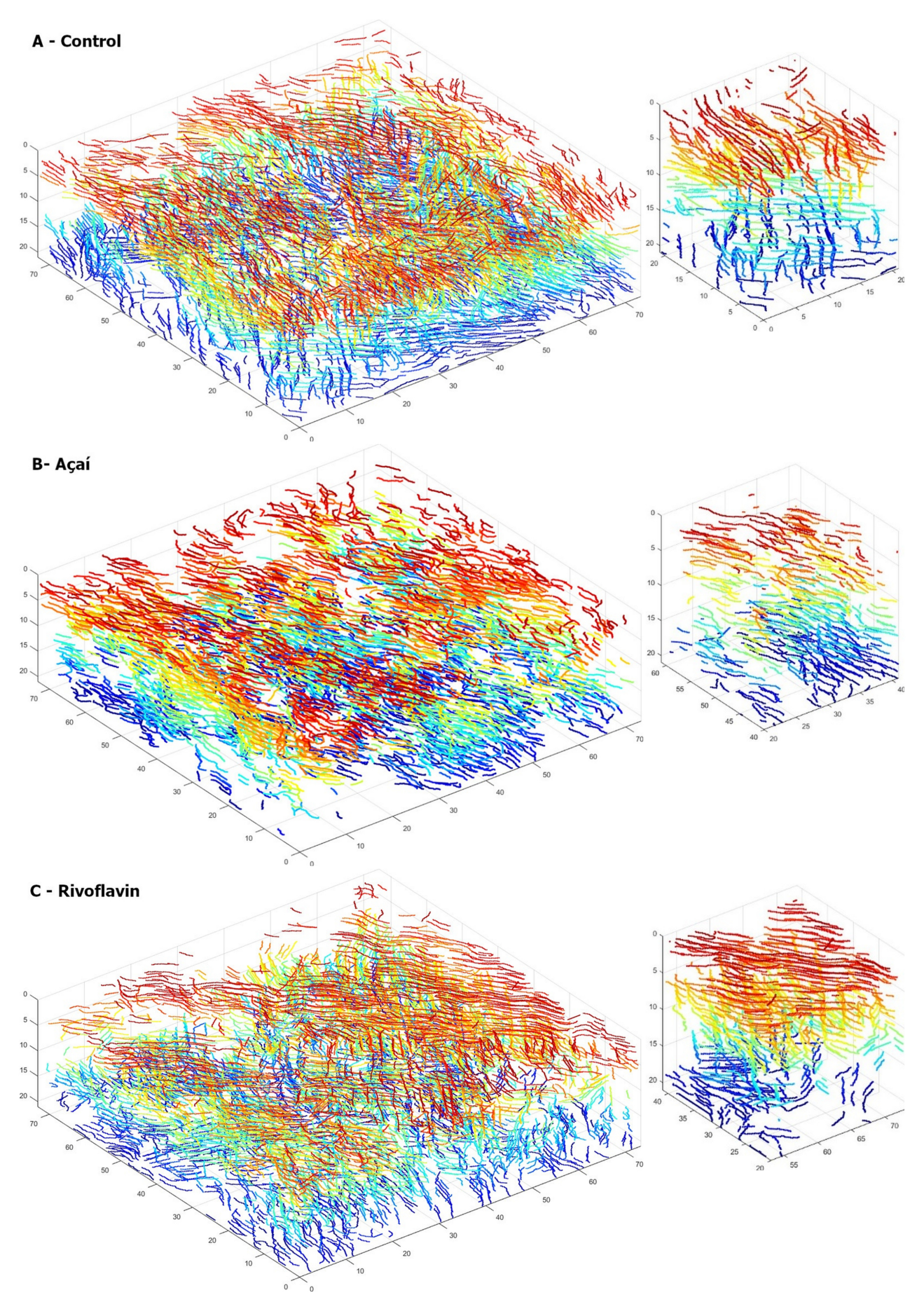


Figure 5